*Journal of Geophysical Research – Solid Earth*

Supporting Information for

# Shallow gas hydrate accumulation at a Nigerian deep-water pockmark - Quantities and dynamics

Thomas Pape[1*], Livio Ruffine[2], Wei-Li Hong[3,4], Nabil Sultan[2], Vincent Riboulot[2], Carl A. Peters[1,††], Martin Kölling[1], Matthias Zabel[1], Sébastien Garziglia[2], Gerhard Bohrmann[1]

[1] MARUM – Center for Marine Environmental Sciences, University of Bremen, Leobener Strasse, 28359 Bremen, Germany

[2] IFREMER, Département Ressources physiques et Ecosystèmes de fond de Mer (REM), Unité des Géosciences Marines, 29280 Plouzané, France

[3] CAGE - Centre for Arctic Gas Hydrate, Environment and Climate, Department of Geology, UiT The Arctic University of Norway, Tromsø, Norway

[4] Geological Survey of Norway, Marine Geology, Trondheim, Norway

[†] now at: Department of Geological Sciences, Stockholm University

[††] now at: Saint Mary's University, Department of Geology, 923 Robie Street, Halifax, NS B3H 3C3, Canada

## Contents of this file



## Introduction

This file contains additional data related to seafloor investigations and sampling during ship expedition GUINECO-MeBo with RV 'Pourquoi pas?' in 2011, descriptions of analytical methods and the numerical model, as well as additional supporting results. Relevant data are also made available through the World Data Center PANGAEA® (www.pangaea.de).

## 1. Lithological and geochemical characteristics of sediment cores

**Table S1.** Sediment texture, gas hydrate fabric and chloride anomalies in gravity cores (code GMGCXX), Calypso cores (code GMCSXX) and MeBo cores (code GMMBXX) next to pressure cores (for core positions refer to Figure 1).

| Pressure core | Proximate sediment core | Fabric of gas hydrates in nearby core | Sediment texture (hydrate-related) | $Cl^-$ concentration anomalies (hydrate-related) | Approx. depth $SO_4^{2-}$ penetration | Depth $CH_4$ concentration maximum |
|---|---|---|---|---|---|---|
| GMDA | | | [m] | [m] | [m] | [m] |
| **01** | | | | slight freshening downwards | 0.30 | |
| | GMGC01 | | 1.10-1.30 moussy, 1.65-2.00 moussy | n.det. | 0.65 | n.det. |
| | GMGC02 | | 0.85-1.10 moussy | n.det. | n.a. | n.det. |
| | GMGC19 | 0.85-1.10 finely disseminated GH | 0.85-1.10 moussy | n.det. | n.a. | n.det. |
| | GMGC34 | | 0.60-1.00 moussy, 1.40-1.80 moussy | n.det. | n.a. | n.det. |
| | GMGC35 | throughout core finely disseminated, platy GH | 0.70-3.20 moussy, 0.80-1.20 soupy, 1.90-2.10 soupy , 2.90 soupy | n.det. | n.a. | n.det. |
| **02** | | | | slight freshening downwards | 0.50 | |
| | GMGC09 | | 1.00-2.40 soupy | n.det. | n.a. | n.det. |
| | GMGC33 | | 0.33-1.00 moussy | n.det. | n.a. | n.det. |
| | GMMB06/07 | | GMMB06: 278-290, 525-555, 555-615 soupy<br>GMMB07: 0-20, 355-380, 490-510, 528-537, 552-558, 648-759, 815-855, 885-895 soupy | GMMB06: >3.40<br>GMMB07: >2.85 | GMMB06: ca. 2.50<br>GMMB07: ca. 1.40 | n.det. |
| | GMMB11 | | 7.40-8.43, 10.85-12.21, 12.29-12.58 moussy/soupy | positive chloride anomaly >6.69 | n.det. | |
| **03** | | | | negative chloride anomaly 0.30-0.90 | 0.30 | |
| | GMGC20 | 0.65-0.80 platy GH; 1.00-1.80 GH layers | 0.80-1.00 moussy, 1.00-1.80 soupy | n.det. | n.a. | n.det. |
| | GMMB10 | | 2.28-2.56, 4.15-4.62, 5.20-5.94, 6.08-6.25, 6.35-7.19, 7.45-7.88, 8.40-8.54, 8.73-9.05, 9.92-10.14, 10.62-10.94, 11.32-12.83, 13.21-13.83, 19.15-20.10, 21.50-21.83 moussy/soupy | >5.15 | ca. 1.50 | 2.46 |

n.det. = not determined

**Table S1 (continuation).** Sediment texture, gas hydrate fabric and chloride anomalies in gravity cores (code GMGCXX), Calypso cores (code GMCSXX) and MeBo cores (code GMMBXX) next to pressure cores (for core positions refer to Figure 1).

| Pressure core | Proximate sediment core | Fabric of gas hydrates in nearby core | Sediment texture (hydrate-related) | $Cl^-$ concentration anomalies (hydrate-related) | Approx. depth $SO_4^{2-}$ penetration | Depth $CH_4$ concentration maximum |
|---|---|---|---|---|---|---|
| GMDA | | | [m] | [m] | [m] | [m] |
| **04** | | | | negative chloride anomaly > 0.70 | 0.50 | |
| | GMGC17 | 3.40 GH pieces | 1.00-2.90 moussy, soupy, 2.10-3.20 moussy, 320-350 soupy | n.det. | n.a. | n.det. |
| | GMGC10 | 0.80-1.00 GH chips; 1.85-2.20 GH chips disseminated | 0.80-1.00 moussy, 1.85-2.20 moussy | n.det. | 0.65 | n.det. |
| **05** | | | | no anomaly | 1.25 | |
| | GMMB08 | | 2.31-2.52, 5.05-5.37, 5.51-6.25, 7.40-9.85, 10.07-10.30, 11.16-11.39, 12.70-12.96, 13.06-13.43, 13.67-13.73, 15.21-15.38, 15.85-15.95, 18.30-18.49, 32.60-32.74, 34.66-34.86 moussy/soupy | >5.35 | n.a. | 6.55 |
| **06** | GMMB08 | | see entry above | >5.35 | n.a. | 6.55 |

n.det. = not determined

## 2. Geochemical modeling

## 2.1 Geochemical modeling of chloride concentrations

**Text S1.** ***Gas hydrate stability and saturation***

As the kinetic model using chloride concentrations is only applicable to the GHSZ, the temperature and pressure regimes where hydrate is stable (gas hydrate equilibrium, GHEQ) have to be determined for each study site. For this the formulation by Tishchenko et al. (2005) and the geothermal gradient reported by Wei et al. (2015) were used. The GHEQ was calculated with three geothermal gradients (72, 112, and 258°C $km^{-1}$). The resulting depths of the GHSZ of 132.5, 82.5, and 34 mbsf, respectively, matched those estimated by Wei et al. (2015, 130 to 35 mbsf).

Methane solubility (MSol) is a function of temperature, pressure, and salinity in the pore water (Sloan and Koh, 2008). In this study the theoretical MSol was determined prior to the model run with the thermodynamic model CSMGem (Sloan and Koh, 2008). Subsequently, the kinetic model retrieves the hydrate stability information through a look-up table approach. MSol was estimated for pore water salinity ranging from fresh water conditions to those doubling typical seawater values (ca. 0.07 kg $kg^{-1}$); a range that covers the observed chloride concentrations (see chapter 4.3 and Wei et al. (2015)). As the model requires input of salinity while only chloride concentrations were measured, salinity was converted to chloride concentration using the empirical equation reported in Peszynska et al. (2016). For simplification of calculations, pressure was set to be constant (11.55 MPa corresponding to water depth of ca. 1,155 mbsl) and six temperature points were used in the estimation of MSol. For each temperature point, a 1$^{st}$ order linear regression was done between MSol and salinity (Figure S1). The slope and intercept, i.e. MSol in fresh water, were used to construct such look-up table for the kinetic model.

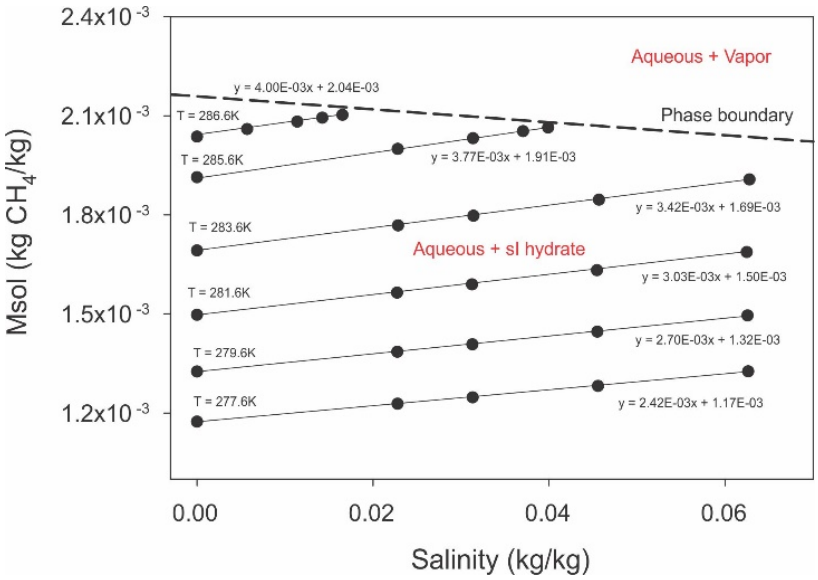


**Figure S1.** Theoretical methane solubility (MSol) as a function of temperature and pore water salinity. Pressure set to be constant (11.55 MPa).

**Text S2.** ***Selection of study sites and sediment properties***

Identical porosity profiles at all sites were assumed, which appears reasonable if porosity data for stations inside and outside the seafloor depression are compared (Figure S2). For the uppermost ~ 60 meters of sediment, the porosity profiles as determined for cores GMMB01/02 and GMMB08 matched with an exponential equation (porosity $\theta = 0.2\ e^{-0.04\ depth} + 0.65$; $R^2 = 0.53$).

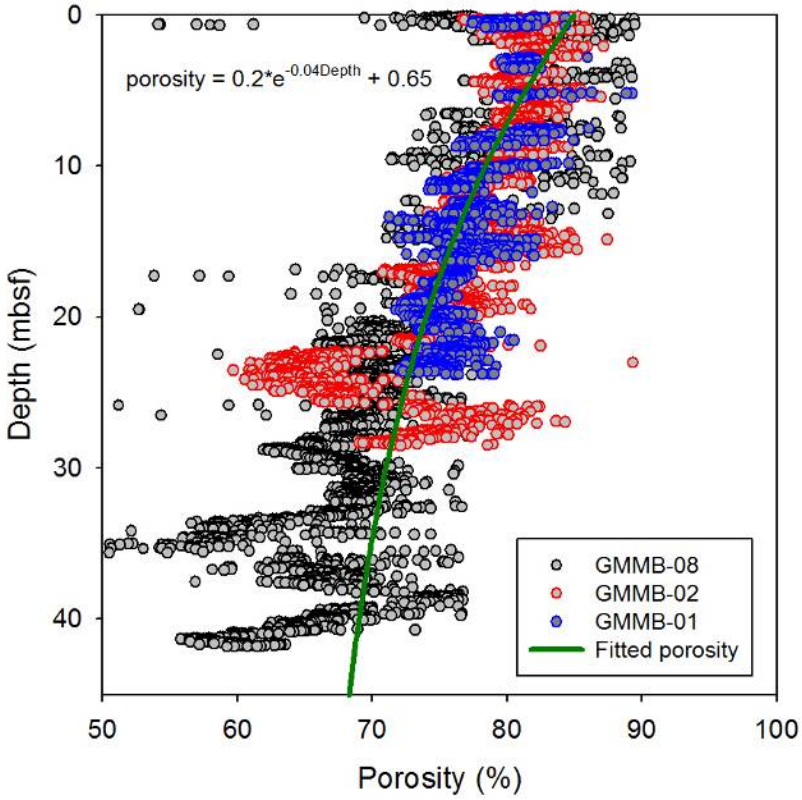


**Figure S2.** Sediment porosity $\theta$ versus sediment depth for MeBo cores GMMB01/02 and GMMB08 as well as best fit equation. Note: For calculations of gas hydrate saturations in pressure cores (chapter 3.4), average porosities of 83%, as well as minimum (75%) and maximum (90%) porosities in sediments above ~5 mbsf were considered.

For all sites investigated, the uppermost 53 m of sediments were modeled except for site GMMB10, which was assumed to have the highest geothermal gradient (see Wei et al. 2015). For that core, only the uppermost 34 meters, which should cover the GHSZ assuming a geothermal gradient of 258°C $km^{-1}$, were modeled. For all other cores, the length and time of the model were discretized by 0.5 m and 0.1 years (yrs), respectively. Such values were determined by running the model with progressing small grid size and time step until stable results were achieved. For modeling GMMB10, smaller spatial and temporal steps (0.321 m and 0.05 yrs), were chosen. The depth ranges where a methane source was added in the model are listed in Table S2. Regardless of depth and site, permeability was assumed to be constant ($10^{-14}$ $m^2$) for pelagic clay (Spinelli et al., 2004). Essential model parameters are summarized in Table S2.

**Table S2.** Essential parameters used for chloride concentration modeling. Bottom sea water temperature as water temperature 50 m above seafloor and geothermal gradients taken from (Wei et al., 2015).ediment texture, gas hydrate fabric and chloride anomalies in gravity cores (code GMGCXX), Calypso cores (code GMCSXX) and MeBo cores (code GMMBXX) next to pressure cores (for core positions refer to Figure 1).

| | Unit | GMMB03 | GMMB12 | GMMB10 | GMMB06/07/11 | GMMB08 |
|---|---|---|---|---|---|---|
| Water depth | mbsl | 1,148 | 1,144 | 1,145 | 1,146 | 1142 |
| Bottom sea water temperature | °C | 4.53 | 4.53 | 4.45 | 4.46 | 4.46 |
| Geothermal gradient | °C $km^{-1}$ | 72 | 72 | 258 | 112 | 112 |
| Length of model | m | 53 | 53 | 34 | 53 | 53 |
| Depth range of additional $CH_4$ input | mbsf | 8 – 18 | 8 – 18 | 5 – 14 | 8 – 18 | 3 – 13 |

**Text S3.** ***Initial and boundary conditions***

For modeling chloride concentration profiles, data from joint cores GMMB01/02 from outside the seafloor depression were used as the initial and boundary conditions. Chloride concentrations gradually decreased from seawater values (555 mM) to 532 mM at 51.7 mbsf. Low chloride concentrations at about 43.8 and 53.0 mbsf in this profile were ignored since they were assumed to reflect gas hydrate dissociation and may therefore not representative of an initial condition with no gas hydrate. Initial absence of methane followed by weak methane supply from the bottom of these cores was assumed as there is no sign of gas hydrate at such depths (Wei et al., 2015).

**Text S4**. ***Advection rate***

For modeling chloride concentration profiles, a compaction-derived fluid advection with a rate of 1.7 x $10^{-4}$ m $yr^{-1}$, estimated from the porosity profile and sediment burial rate of ca. 2 x $10^{-4}$ m $yr^{-1}$ (Riboulot et al., 2012) only was assumed. Application of such advection rate in the model resulted in a good fit with the observed chloride profiles from GMMB01/02 (Figure S3).

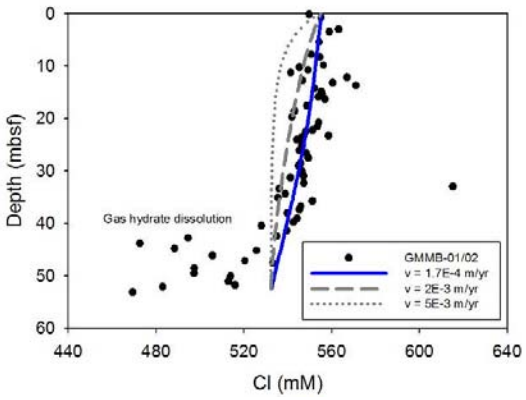


**Figure S3.** Recalculated pore water chloride concentrations vs. depth at GMMB01/02 outside of the seafloor depression and best fit equation considering various fluid advection rates.

## 2.2 Geochemical modeling of sulfate concentrations

**Table S3.** Parameters used in the numerical model for sulfate concentrations.

| Parameter | Symbol | Unit | GMMB01/02 | GMMB03 | GMMB12 |
|---|---|---|---|---|---|
| Model domain | L | M | 75 | 6.9 | 6.7 |
| Molecular diffusion coefficient, $SO_4$ | $D_{SO4}$ | $m^2\ sec^{-1}$ | 5.51E-10 | 5.51E-10 | 5.51E-10 |
| Molecular diffusion coefficient, $CH_4$ | $D_{CH4}$ | $m^2\ sec^{-1}$ | 8.62E-10 | 8.62E-10 | 8.62E-10 |
| $SO_4$ conc. at sediment surface | $[SO_4]$ | mM | 28.7 | 28.7 | 28.7 |
| $CH_4$ conc. at sediment surface | $[CH_4]$ | mM | 0 | 0 | 0 |
| $CH_4$ conc. at lower boundary domain | $[CH_4]$ | mM | 66 | 66 | 66 |
| $SO_4$ flux at lower boundary domain | $\frac{\partial[SO_4]}{\partial x}\Big)_L$ | $mM\ m^{-1}$ | 0 | 0 | 0 |
| Upward fluid velocity | v | $m\ yr^{-1}$ | 0 | 0 | 0 |
| AOM constant rate | $k_{AOM}$ | $mM^{-1}\ yr^{-1}$ | 3E-02 | 3E-02 | 3E-02 |

Note: Model domains at each site are determined from extrapolation of the upper sections of the sulfate profile as proposed by Fischer et al (2013).

## 2.3. Density of porous gas hydrates

**Text S5.** ***Density calculations of porous gas hydrates***

Bulk densities of porous hydrates recovered from the southern summit of Hydrate Ridge at about 780 mbsl ranged between ca. 0.2 and 0.6 g $cm^{-3}$, with most values clustering around 0.4 g $cm^{-3}$ (Suess et al., 2001). The authors additionally estimated the pore volume of such hydrates to be approximately 60 vol%. Similar *in situ* densities might also be applied for the porous hydrate specimen recovered from Pockmark A. While the density of sI hydrate is approximately 0.910 g $cm^{-3}$ (Davidson, 1981; Koh, 2002), that of free methane at *in situ* conditions (hydrostatic pressure: 11.4 MPa, temperature: 277.55K) is ca. 0.099 g $cm^{-3}$ (www.pipeng.com/index.php/tsps/itdtoflup00401/%29). Then, the bulk density of porous hydrates at Pockmark A comprising an average pore volume of 60 vol% would be 0.42 g $cm^{-3}$. Moreover, the calculated *in situ* density of bottom sea waters at Pockmark A is 1.0327 g $cm^{-3}$ (*S* = 34.59; http://www.phys.ocean.dal.ca/~kelley/seawater/density.html), while the wet bulk density of non-hydrate bearing diatomaceous clays forming surface deposits at the nearest ODP Site (Holes 1075 and 1076) was reported to be about 1.19 g $cm^{-3}$ (Wefer et al., 1988). Provided that the bottom sea water density and pore water density in the surface sediments at Pockmark A are equal, then a proportion of ≥20 vol% of such porous gas hydrate in a unit cell of sediment would result in a bulk (porous gas hydrate + wet sediment) density that is lower than that of bottom sea water. Pore water chloride enrichments ($Cl^-$ up to 960 mM; *S* = 67.89) observed in several MeBo cores (Figure 3c) results in higher pore water densities (1.0591 g $cm^{-3}$) and higher fractions of porous hydrate (≥24 vol%) required to induce buoyant hydrate uplift.

## 3 Results

### 3.1 Molecular compositions of light hydrocarbons and stable isotopic compositions of methane

**Table S4.** Molecular hydrocarbon composition (expressed as $C_1/C2_+$ ratio) of gas hydrates and stable carbon and hydrogen isotope ratios of hydrate-bound methane prepared from gravity cores and MeBo cores.

| Internal core code | Supplementary core code ('Pangaea') | Sample # (GC), Barrel no. (MeBo) | Section depth of hydrate samples analyzed [cmbsf] | $C_1/C_{2+}$ | $\delta^{13}C\text{-}CH_4$ [‰ V-PDB] | $\delta^{2}H\text{-}CH_4$ [‰ SMOW] |
|---|---|---|---|---|---|---|
| GMGC01 | 16001-1 | | 110–130, 165–200 | 6,556 | –51.1 | –179.5 |
| GMGC02 | 16001-2 | | 85–110 | 3,339 | –51.4 | –182.1 |
| GMGC10 | 16012-1 | | 80–220 | 6,594 | –51.7 | –179.4 |
| GMGC12 | 16013-2 | 1 | n.doc. | 3,089 | –50.5 | –179.6 |
| GMGC12 | 16013-2 | 2 | n.doc. | 7,674 | –50.4 | –182.9 |
| GMGC17 | 16022-1 | | 350 | 8,443 | –51.0 | –180.9 |
| GMGC20 | 16025-1 | | 80 | 6,461 | –51.0 | –179.1 |
| GMGC28 | 16040-1 | | 340–410 | 8,050 | –51.2 | –179.5 |
| GMGC30 | 16043-1 | | 140–230 | 6,366 | –50.9 | –180.7 |
| GMGC32 | 16044-2 | | 105–120 | 3,212 | –51.0 | n. anal. |
| GMGC33 | 16045-1 | 1 | 33–100 | 8,892 | –53.4 | n. anal. |
| GMGC33 | 16045-1 | 2 | 33–100 | 8,892 | –53.2 | n. anal. |
| GMGC35 | 16046-2 | | 290 | 8,557 | –51.2 | n. anal. |
| GMGC36 | 16046-3 | | n.doc. | 14,900 | –50.9 | n. anal. |
| GMGC38 | 16046-4 | | n.doc. | 15,940 | –50.2 | n. anal. |
| | | | | | | |
| GMMB03 | 16010-1 | 5P | 975–1,231 | 5,106 | –50.0 | –178.3 |
| GMMB03 | 16010-1 | 6P | 1,231–1,481 | 4,760 | –50.7 | –178.4 |
| GMMB07 | 16028-1 | 4P | 775–1,019 | 5,116 | –50.3 | –181.4 |
| GMMB10 | 16036-1 | 5P | 745–992 | 3,796 | –50.3 | –179.1 |
| GMMB11 | 16042-1 | 5P | 740–843 | 6,394 | –49.5 | n. anal. |
| GMMB12 | 16049-1 | 6P | 989–1,248 | 23,839 | –49.4 | n. anal. |

n.doc. = not documented; n. anal. = not analyzed

## 3.2 Simulation of heat propagation in surface sediments induced by bottom sea water warming

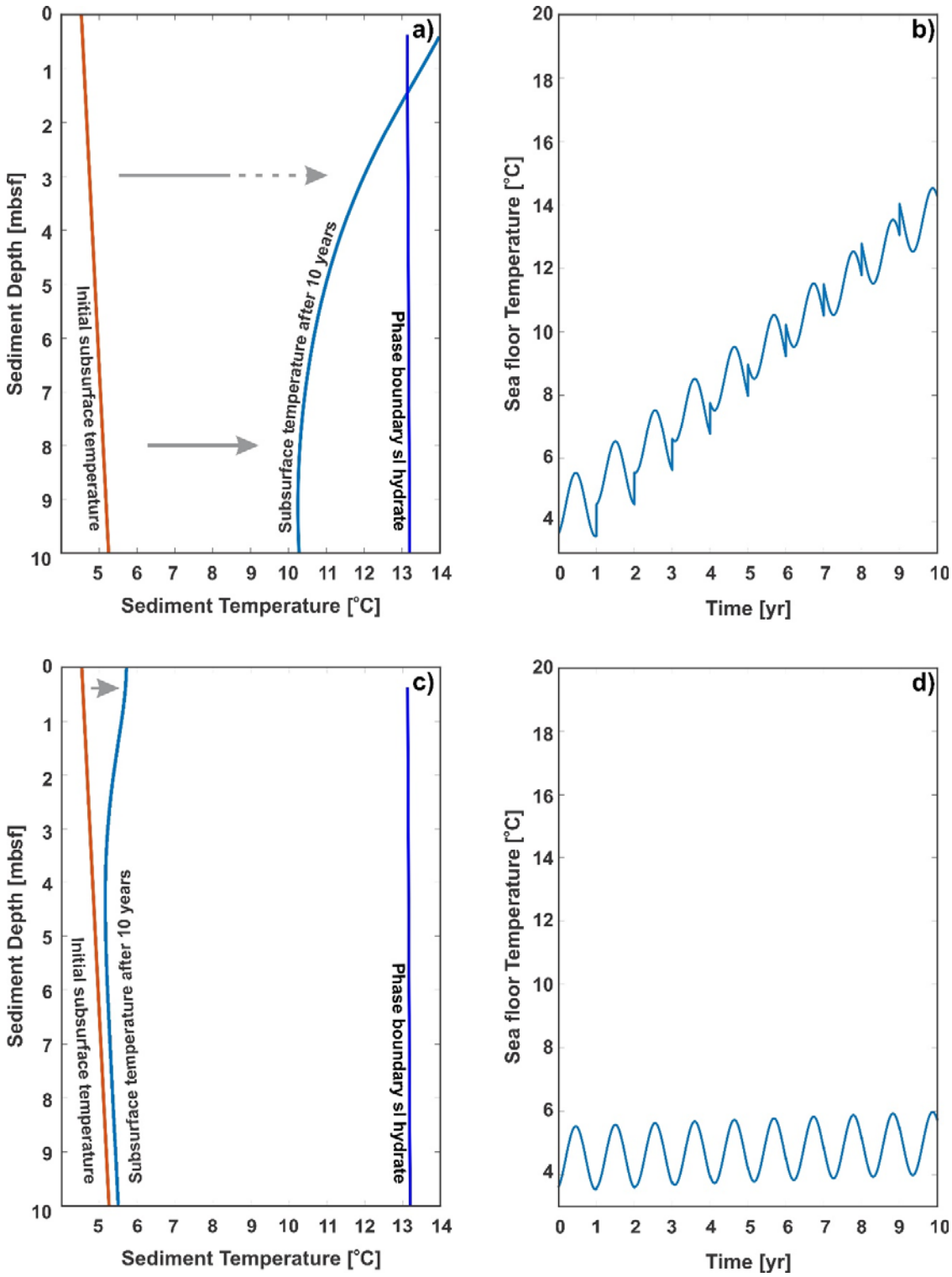

**Figure S4** (previous page)**.** Model results of heat propagation from bottom sea water into the sediments at Pockmark A induced by a hypothetical bottom sea water warming in order to evaluate potential dissociation of gas hydrates present in uppermost sediments. Model parametrization as described in Hong et al. (2017).
a) Sediment temperature (in °C, light blue line) vs. sediment depth (in meters below seafloor, mbsf). Brown line: initial temperature in the seabed (temperature gradient 72 °C $km^{-1}$), dark blue line: Phase boundary for sI hydrates (Wei et al., 2015). The model was started at current sediment and bottom sea water temperature and hydrostatic pressure conditions. Because modeling was done for a very short time scale (10 years), variations in sediment thickness were considered irrelevant. Sediment temperatures exceeding gas hydrate dissociation temperatures causing dissociation of gas hydrate in the uppermost approximately 1.5 meters of sediment are only achieved when bottom sea water temperature is increased at an extreme rate of 1.0 °C $yr^{-1}$ for a time period of 10 years. For gradual evolution of the sediment temperature refer to file 'modelmovie.avi' in the Supporting Information.
b) Time vs. hypothetical increase of bottom sea water temperature at a rate of 1.0 °C $yr^{-1}$.
c) Sediment temperature (in °C, light blue line) vs. sediment depth (in meters below seafloor, mbsf). Initial temperature in the seabed (brown line; temperature gradient 72 °C $km^{-1}$) and phase boundary for sI hydrates (dark blue line) as in Figure S4a. The model was run with an increase in bottom sea water temperature by 0.05 °C $yr^{-1}$, which is more realistic at the deep-water Pockmark A than the temperature increase of 1.0 °c $yr^{-1}$ illustrated in Figure S4a. After ten years of bottom water increase, sediment temperatures are still > 7°C lower than gas hydrate dissociation temperatures.
d) Time vs. hypothetical increase of bottom sea water temperature at a rate of 0.05 °C $yr^{-1}$.